NASA/TM–20230002114

A THEORETICAL AND COMPUTATIONAL REVISIT OF CONVERSIONS BETWEEN WHITHAM'S F-FUNCTION AND EQUIVALENT AREA

Wu Li
Aeronautics Systems Analysis Branch
NASA Langley Research Center, Hampton, Virginia

May 2023

NASA STI Program Report Series

The NASA STI Program collects, organizes, provides for archiving, and disseminates NASA's STI. The NASA STI program provides access to the NTRS Registered and its public interface, the NASA Technical Reports Server, thus providing one of the largest collections of aeronautical and space science STI in the world. Results are published in both non-NASA channels and by NASA in the NASA STI Report Series, which includes the following report types:

- TECHNICAL PUBLICATION. Reports of completed research or a major significant phase of research that present the results of NASA Programs and include extensive data or theoretical analysis. Includes compilations of significant scientific and technical data and information deemed to be of continuing reference value. NASA counter-part of peer-reviewed formal professional papers but has less stringent limitations on manuscript length and extent of graphic presentations.

- TECHNICAL MEMORANDUM. Scientific and technical findings that are preliminary or of specialized interest, e.g., quick release reports, working papers, and bibliographies that contain minimal annotation. Does not contain extensive analysis.

- CONTRACTOR REPORT. Scientific and technical findings by NASA-sponsored contractors and grantees.

- CONFERENCE PUBLICATION. Collected papers from scientific and technical conferences, symposia, seminars, or other meetings sponsored or co-sponsored by NASA.

- SPECIAL PUBLICATION. Scientific, technical, or historical information from NASA programs, projects, and missions, often concerned with subjects having substantial public interest.

- TECHNICAL TRANSLATION. English-language translations of foreign scientific and technical material pertinent to NASA's mission.

Specialized services also include organizing and publishing research results, distributing specialized research announcements and feeds, providing information desk and personal search support, and enabling data exchange services.

For more information about the NASA STI program, see the following:

- Access the NASA STI program home page at http://www.sti.nasa.gov

- Help desk contact information:

https://www.sti.nasa.gov/sti-contact-form/ and select the "General" help request type.

NASA/TM–20230002114

A THEORETICAL AND COMPUTATIONAL REVISIT OF CONVERSIONS BETWEEN WHITHAM'S F-FUNCTION AND EQUIVALENT AREA

Wu Li
Aeronautics Systems Analysis Branch
NASA Langley Research Center, Hampton, Virginia

National Aeronautics and
Space Administration

Langley Research Center
Hampton, Virginia 23681-2199

May 2023

Acknowledgments

This work is funded by the NASA Commercial Supersonic Technology Project. The author is sincerely thankful to Mark Guynn at NASA's Langley Research Center for his valuable and constructive comments that have led to a significant improvement in the original paper.

Available from:

NASA Center for Aerospace Information
7115 Standard Drive
Hanover, MD 21076-1320
443-757-5802

List of Symbols

Term	Description
$\boldsymbol{A}(\cdot)$	operator to denote the inverse Abel transform from F to A_e
$\boldsymbol{A}(F)$	A_e converted from F using $\boldsymbol{A}(\cdot)$, ft^2
$\boldsymbol{A}\circ\boldsymbol{F}$, $\boldsymbol{F}\circ\boldsymbol{A}$	composition of two integral transforms: $\boldsymbol{A}\circ\boldsymbol{F}(A_e) = \boldsymbol{A}(\boldsymbol{F}(A_e))$, $\boldsymbol{F}\circ\boldsymbol{A}(F) = \boldsymbol{F}(\boldsymbol{A}(F))$
A_e	equivalent area for a body of revolution, ft^2
A'_e	first derivative of A_e with respect to x_e
A''_e	second derivative of A_e with respect to x_e
A''_i	approximate value of $A''_e(x_i)$
$\boldsymbol{A}_N(\cdot)$	operator to denote the numerical transform from F to A_e as an approximation of $\boldsymbol{A}(\cdot)$
$\boldsymbol{A}_N(F)$	numerical approximation of $\boldsymbol{A}(F)$, ft^2
F, $F(x_e)$	Whitham's F-function
F'	first derivative of F with respect to x_e
$\boldsymbol{F}(\cdot)$	operator to denote the Whitham integral transform from A_e to F
$\boldsymbol{F}(A_e)$	F converted from A_e using $\boldsymbol{F}(\cdot)$
F_i, F_k	notations for $F(x_i)$, $F(x_k)$
f_N, $f_N(x_e)$	notations to represent $\boldsymbol{F}_N(A_e)$ as a function of x_e
$\boldsymbol{F}_N(\cdot)$	operator to denote the numerical transform from A_e to F as an approximation of $\boldsymbol{F}(\cdot)$
$\boldsymbol{F}_N(A_e)$	numerical approximation of $\boldsymbol{F}(A_e)$
g, G	notations for functions
g', g''	first and second derivatives of g
i, j, k, n, N	integers
l_e	effective length of supersonic configuration, which is the largest effective distance where Mach angle cut plane intersects the configuration, ft
t,u,θ	temporary variables
x, y, z	coordinates of point in space, ft
$x_{c,j}$, $y_{c,j}$	(x,y) coordinates of a control point of a Bezier curve, ft
x_e	effective distance for A_e and F, ft
x_i	end point of a linear segment of a piecewise linear approximation function, ft
$\Delta A''_i$	$A''_i - A''_{i-1}$
ΔF_i	$F_i - F_{i\text{-}1}$
Δx_i	$x_i - x_{i\text{-}1}$
σ	positive number
τ	positive constant as an upper bound for $\lvert A''_e \rvert$

Abstract

This paper proves mathematically that the integral transforms between Whitham's F-function and equivalent area are the inverse transforms of each other if and only if the slope of the equivalent area at the origin is zero. This mathematical fact contradicts the accepted unconditional inverse relation between Whitham's F-function and equivalent area in the sonic boom research literature. Piecewise linear approximations of an F-function and of the second derivative of an equivalent area are used to derive numerical formulas for conversions between Whitham's F-function and equivalent area. Numerical results are included to show convergence of the numerical conversions as the maximum length of the segments for piecewise linear approximations goes to zero. These numerical conversions are approximately the inverse transforms of each other when the second derivative of an equivalent area is continuous and the slope of the equivalent area at the origin is zero.

1 Introduction

The Whitham theory [1,2] on the equivalent body of revolution for a supersonic configuration is the basis for the sonic boom minimization theory by Seebass and George [3]. Darden [4] extended the George-Seebass sonic boom minimization theory from an isothermal atmosphere to the real atmosphere. The George-Seebass-Darden (GSD) sonic boom minimization theory was widely used in the sonic boom minimization studies before the Shaped Sonic Boom Demonstration (SSBD) program and led to a measured flat-top ground signature of the SSBD demonstrator [5]. For historical accounts of sonic boom research using the theory of equivalent body of revolution, see Refs. [6-13]. In contrast, the state-of-the-art sonic boom analysis [14,15] computes the off-body pressure at three body lengths away from the aircraft using computational fluid dynamics (CFD) and propagates the off-body pressure to the ground using an augmented Burgers equation. This is the analysis method for an early version of the NASA X-59 low-boom flight demonstrator [14,16], which aims to enable a commercially successful supersonic transport to fly overland with a quiet sonic thump, rather than a loud sonic boom, on the ground. Typically, a supersonic configuration and its equivalent body of revolution can have significantly different aft signature shapes. However, the Whitham theory is still useful when the equivalent body of revolution for a supersonic configuration is corrected using the CFD off-body pressure. The supersonic configuration and its corrected equivalent body of revolution have approximately the same undertrack sonic boom ground signature. The corrected equivalent body of revolution is defined by the reversed equivalent area of a supersonic configuration [17]. Designing a low-boom supersonic configuration is equivalent to designing a low-boom reversed equivalent area shape. See Ref. [18] for a theoretical justification of this statement. The reversed equivalent area enables a multiobjective multidisciplinary optimization (MDO) method, called the Block Coordinate Optimization method, for conceptual design of low-boom supersonic transports that can satisfy both the low-boom and mission performance requirements [19,20]. The integral transform from an equivalent area to Whitham's F-function is an important analysis step for finding optimal equivalent area targets for inverse design optimization of the reversed equivalent area of a supersonic aircraft [19,20]. The accuracy of numerical methods for conversions between Whitham's F-function and equivalent area needs to be carefully studied in the new application setting.

This paper restudies Whitham's F-function, denoted by $F(x_e)$, and the corresponding equivalent area, denoted by $A_e(x_e)$, from mathematical and computational perspectives. Here x_e represents the effective distance to define the Mach angle cut plane used for calculation of $A_e(x_e)$. The inverse relations between the Whitham integral transform [1,2] from $A_e(x_e)$ to $F(x_e)$ and its Abel inversion from $F(x_e)$ to $A_e(x_e)$ [3] will be rigorously reexamined. Carlson [21] developed a numerical integration procedure for converting $A_e(x_e)$ to

$F(x_e)$. Carlson's numerical approximation of $F(x_e)$ is obtained by replacing $A_e''(x_e)$ with a piecewise constant approximation of $A_e''(x_e)$, which is equivalent to a piecewise quadratic polynomial approximation of $A_e(x_e)$. Igoe [22] studied a specific case of Carlson's method and derived an approximation error estimate using the third and fourth derivatives of $A_e(x_e)$. Using a general piecewise polynomial approximation of $A_e(x_e)$, Ritzel and Gottlieb [23] derived a more general numerical approximation formula for converting $A_e(x_e)$ to $F(x_e)$ and stated that the proposed numerical approximation formula is as accurate as Igoe's formula. In this paper, a piecewise linear approximation of $A_e''(x_e)$ is used to convert $A_e(x_e)$ to $F(x_e)$. Moreover, a numerical formula for converting $F(x_e)$ to $A_e(x_e)$ is also provided using a piecewise linear approximation of $F(x_e)$. The accuracies of these numerical formulas and the inverse relations between the numerical conversions will be verified computationally.

To provide a succinct description of the main results in this paper, operator notations for the integral transforms between $A_e(x_e)$ and $F(x_e)$ are introduced. The Whitham integral transform from $A_e(x_e)$ to $F(x_e)$ is denoted by an operator $\boldsymbol{F}(\cdot)$, i.e., $F = \boldsymbol{F}(A_e)$. The inverse Abel transform from $F(x_e)$ to $A_e(x_e)$ is denoted by $\boldsymbol{A}(\cdot)$, i.e., $A_e = \boldsymbol{A}(F)$. Mathematical proofs will be provided to establish the necessary and sufficient boundary condition of $A_e(x_e)$ for the inverse relations $\boldsymbol{A}\circ\boldsymbol{F}(A_e) = A_e$ and $\boldsymbol{F}\circ\boldsymbol{A}(F) = F$. In particular, if $A_e'(0) \neq 0$ (e.g., the equivalent area of a blunt-tipped projectile), then $\boldsymbol{A}\circ\boldsymbol{F}(A_e) \neq A_e$, i.e., $\boldsymbol{A}(F)$ is not mathematically an inverse transform of $F = \boldsymbol{F}(A_e)$. This contradicts the accepted conclusion in the sonic boom research literature that $\boldsymbol{A}\circ\boldsymbol{F}(A_e) = A_e$ is always true.

For a finite set of x_e locations, $0 = x_0 < x_1 < \ldots < x_N$, the proposed numerical conversion from $A_e(x_e)$ to $F(x_e)$ is denoted by an operator $\boldsymbol{F}_N(\cdot)$, and $\boldsymbol{F}_N(A_e)$ is the numerical approximation of $F(x_e)$ using a piecewise linear approximation of $A_e''(x_e)$. Similarly, the proposed numerical conversion from $F(x_e)$ to $A_e(x_e)$ is denoted by $\boldsymbol{A}_N(\cdot)$, and $\boldsymbol{A}_N(F)$ is the numerical approximation of $A_e(x_e)$ using a piecewise linear approximation of $F(x_e)$. Here a piecewise linear approximation means that the approximation function is a linear function on each subinterval $[x_{i-1}, x_i]$ and the subscript N indicates that the numerical conversions depend on the number of partition points. However, at the boundaries of the effective distance range, $x_e = 0$ and $x_e = l_e$, the piecewise linear approximation of $A_e''(x_e)$ must be replaced by piecewise constant approximations so that $\boldsymbol{F}_N(A_e)$ will be accurate even if $A_e'(0) \neq 0$ or $A_e'(l_e) \neq 0$. In theory, $\boldsymbol{F}_N(A_e)$ is very different from Carlson's numerical approximation of $\boldsymbol{F}(A_e)$ [21]. In application, $\boldsymbol{F}_N(A_e)$ is nearly identical to Carlson's numerical approximation of $\boldsymbol{F}(A_e)$ with an appropriate constant approximation of $A_e''(x_e)$ on each subinterval $[x_{i-1}, x_i]$.

Instead of providing mathematical proofs for $\boldsymbol{F}_N(A_e) \to \boldsymbol{F}(A_e)$ and $\boldsymbol{A}_N(F) \to \boldsymbol{A}(F)$ as N goes to infinity, three numerical examples are provided to illustrate how the numerical approximation errors $|\boldsymbol{F}(A_e)-\boldsymbol{F}_N(A_e)|$, $|A_e-\boldsymbol{A}_N\circ\boldsymbol{F}_N(A_e)|$, $|\boldsymbol{A}(F)-\boldsymbol{A}_N(F)|$, and $|F-\boldsymbol{F}_N\circ\boldsymbol{A}_N(F)|$ behave under different assumptions about the boundedness of $|A_e''(x_e)|$ and the value of $A_e'(0)$. Overall, the numerical approximations $\boldsymbol{F}(A_e) \approx \boldsymbol{F}_N(A_e)$, $F \approx \boldsymbol{F}_N\circ\boldsymbol{A}_N(F)$, $\boldsymbol{A}(F) \approx \boldsymbol{A}_N(F)$, and $A_e \approx \boldsymbol{A}_N\circ\boldsymbol{F}_N(A_e)$ are very accurate for $N \geq 100$ if $A_e''(x_e)$ is continuous on $[0, l_e]$ and $A_e'(0) = 0$. However, if $A_e'(0) \neq 0$, then $\boldsymbol{F}(A_e) \approx \boldsymbol{F}_N(A_e)$ and $\boldsymbol{A}(F) \approx \boldsymbol{A}_N(F)$ with $F = \boldsymbol{F}(A_e)$ are still accurate, but $\boldsymbol{A}_N\circ\boldsymbol{F}_N(A_e)$ converges to $\boldsymbol{A}\circ\boldsymbol{F}(A_e)$, which differs from A_e.

The paper is organized as follows. Mathematical proofs of $\boldsymbol{A}\circ\boldsymbol{F}(A_e) = A_e$ and $\boldsymbol{F}\circ\boldsymbol{A}(F) = F$ under the required boundary condition $A_e'(0) = 0$ are presented in Sec. 2. Numerical formulas for conversions between A_e and F are given in Secs. 3 and 4. Section 5 includes the numerical results to verify the accuracies of the numerical conversions and their inverse relations. The last section has the conclusions.

2 Verification of Inverse Relations

Whitham [1] introduced the F-function in Eq. (1) that can be scaled to predict the pressure distribution around a supersonic projectile with weak shocks. Later, Whitham [2] extended the F-function theory for a thin symmetric wing and Walkden [24] extended Whitham's result to a combination of an axisymmetric body and a wing at a small incident angle with respect to the flow direction.

$$F(x_e) = \boldsymbol{F}(A_e) = \frac{1}{2\pi} \cdot \int_0^{x_e} \frac{A_e''(t)}{\sqrt{x_e - t}} dt \tag{1}$$

In Eq. (1), the integral transform from $A_e(x_e)$ to $F(x_e)$ is denoted by the operator $\boldsymbol{F}(\cdot)$. When $A_e(x_e)$ represents an equivalent body of revolution for a supersonic configuration, $A_e(x_e)$ is defined by the Mach angle cut method {see Ref. [6]} for $x_e \le l_e$, where l_e is the effective length of the supersonic configuration. The values of $F(x_e)$ for $x_e > l_e$ characterize the turbulent wake and the wake is usually modeled as a part of the body using $A_e(x_e) = A_e(l_e)$ for $x_e > l_e$ {see the footnote on page 302 in Ref. [1]}.

Equation (1) is Abel's transform of the first kind for $A_e''(x_e)$. See Ref. [25] for a summary and a comprehensive reference list about Abel's transform of the first kind and its applications. The inverse Abel transform was used to derive the following inverse transform of Eq. (1).

$$A_e(x_e) = \boldsymbol{A}(F) = 4 \cdot \int_0^{x_e} F(t) \cdot \sqrt{x_e - t}\, dt \tag{2}$$

The derivation of Eq. (2) from the inverse Abel transform of Eq. (1) was outlined in Chapter 7 of Ref. [13] and credited to Jones [26]. One implicit assumption in the derivation is that $A_e'(0) = 0$. This was not mentioned in Ref. [13] but is required for the validity of eq. (2) in Chapter 7 of Ref. [13]. George and Seebass [3] developed the sonic boom minimization theory using Eq. (2) as the inverse transform of Eq. (1) for $x_e \le l_e$. The validity of the inverse relations between Eqs. (1) and (2) is based on Abel's work in 1826 {see the first reference in Ref. [25]}. In general, Abel's transform of the first kind and its inverse transform require pairs of functions belonging to a variety of functional spaces {see Ref. [25]}. In this section, the inverse relations between Eqs. (1) and (2) are rigorously proved using some mathematical properties of $A_e(x_e)$ and $F(x_e)$ that are relevant to applications of the Whitham theory for sonic boom minimization.

Theorem 1 (Inversion from Whitham's F-function to Equivalent Area). Assume that (i) $A_e(0) = 0$, (ii) $A_e'(x_e)$ is a continuous function on the interval $[0, l_e]$, (iii) $A_e''(x_e)$ exists everywhere except at a finite number of locations, (iv) $\int_0^{x_e} |A_e''(t)|/\sqrt{x_e - t}\, dt$ is bounded for $0 < x_e \le l_e$, and (v) for any $\sigma > 0$, $|A_e''(x_e)|$ is bounded by a constant for $\sigma \le x_e \le l_e$. Then

(1.1) $\boldsymbol{F}(A_e)$ is continuous and bounded for $0 < x_e \le l_e$.

(1.2) $\boldsymbol{A} \circ \boldsymbol{F}(A_e) = A_e(x_e) - A_e'(0) \cdot x_e$ for $x_e \le l_e$.

(1.3) $\boldsymbol{A} \circ \boldsymbol{F}(A_e) = A_e(x_e)$ for $x_e \le l_e$ if and only if $A_e'(0) = 0$.

Proof. First, the boundedness of $\boldsymbol{F}(A_e)$ for $x_e \le l_e$ follows from Assumption (iv) of Theorem 1. For convenience, we also use $F(x)$ and $A_e(x)$ to represent Whitham's F-function and equivalent area if the physical implication of the variable is not important. Assumption (iv) also implies that $A_e''(x)$ is Lebesgue integrable [27] {see also page 24 in Ref. [28]} on $[0, l_e]$ because

$$\int_0^{l_e} |A_e''(t)| dt \le \sqrt{l_e} \cdot \int_0^{l_e} |A_e''(t)|/\sqrt{l_e - t}\, dt < \infty$$

The continuity of $\boldsymbol{F}(A_e)$ at $x_e > 0$ can be proved by splitting $\int_0^x A_e''(t)/\sqrt{x - t}\, dt$ into the sum of $\int_0^\sigma A_e''(t)/\sqrt{x - t}\, dt$ and $\int_\sigma^x A_e''(t)/\sqrt{x - t}\, dt$ with $0 < \sigma < x_e$. The continuity of $\int_0^\sigma A_e''(t)/\sqrt{x - t}\, dt$ at $x = x_e$ follows from $\int_0^\sigma |A_e''(t)| dt < \infty$ and the uniform continuity of $1/\sqrt{x - t}$ for $0 \le t \le \sigma$ and $(\sigma + x_e)/2 \le x \le \sigma + x_e$. The continuity of $\int_\sigma^x A_e''(t)/\sqrt{x - t}\, dt$ at $x = x_e$ follows from the following error estimate. For convenience, assume $x > x_e$ and $|A_e''(x_e)|$ is bounded by τ for $x_e \ge \sigma$ [see Assumption (v)]. Then, as $x \to x_e$, we have

$$\left|\int_\sigma^x \frac{A_e''(t)}{\sqrt{x-t}}dt - \int_\sigma^{x_e} \frac{A_e''(t)}{\sqrt{x_e-t}}dt\right| = \left|\int_{x_e}^x \frac{A_e''(t)}{\sqrt{x-t}}dt + \int_\sigma^{x_e} A_e''(t)\cdot\left(\frac{1}{\sqrt{x-t}} - \frac{1}{\sqrt{x_e-t}}\right)dt\right|$$
$$\le \int_{x_e}^x \frac{|A_e''(t)|}{\sqrt{x-t}}dt + \int_\sigma^{x_e} |A_e''(t)|\cdot\left(\frac{1}{\sqrt{x_e-t}} - \frac{1}{\sqrt{x-t}}\right)dt$$
$$\le \tau\cdot\int_{x_e}^x \frac{1}{\sqrt{x-t}}dt + \tau\cdot\int_\sigma^{x_e}\left(\frac{1}{\sqrt{x_e-t}} - \frac{1}{\sqrt{x-t}}\right)dt$$
$$= 2\tau\cdot\sqrt{x-x_e} + 2\tau\left(\sqrt{x_e-\sigma} - \sqrt{x-\sigma} + \sqrt{x-x_e}\right) \to 0$$

This proves that the right limit of $\int_\sigma^x A_e''(t)/\sqrt{x-t}\,dt$ at $x = x_e$ is $\int_\sigma^{x_e} A_e''(t)/\sqrt{x_e-t}\,dt$. A similar error estimate can be used to prove that the left limit of $\int_\sigma^x A_e''(t)/\sqrt{x-t}\,dt$ at $x = x_e$ is also $\int_\sigma^{x_e} A_e''(t)/\sqrt{x_e-t}\,dt$. So, $\int_\sigma^x A_e''(t)/\sqrt{x-t}\,dt$ is continuous at $x = x_e$. Because $\int_0^x A_e''(t)/\sqrt{x-t}\,dt$ is the sum of two continuous functions at $x = x_e$, $\int_0^x A_e''(t)/\sqrt{x-t}\,dt$ is also continuous at $x = x_e$. This completes the proof of the continuity of $\boldsymbol{F}(A_e)$ for $0 < x_e \le l_e$. So, $\boldsymbol{F}(A_e)$ is continuous and bounded for $0 < x_e \le l_e$, which is (1.1) of Theorem 1.

Because $A_e'(x)$ is a continuous function on [0, l_e] [see Assumption (ii)], $A_e''(x)$ exists everywhere except at a finite number of locations [see Assumption (iii)], and $A_e''(x)$ is Lebesgue integrable (proved above), by the Fundamental Theorem of Calculus [29] {see also page 148 in Ref. [28]},

$$\int_0^{x_e} A_e''(u)\,du = A_e'(x_e) - A_e'(0) \qquad \text{for any } 0 \le x_e \le l_e \tag{3}$$

Now, we can rewrite $\boldsymbol{A}\circ\boldsymbol{F}(A_e)$ in terms of A_e''. Assume that $F = \boldsymbol{F}(A_e)$ is defined by Eq. (1). Then the following equalities hold for $0 \le x_e \le l_e$.

$$4\cdot\int_0^{x_e} F(t)\cdot\sqrt{x_e-t}\,dt = 4\cdot\int_0^{x_e}\left[\frac{1}{2\pi}\cdot\int_0^t \frac{A_e''(u)}{\sqrt{t-u}}du\cdot\sqrt{x_e-t}\right]dt \quad \text{[use Eq. (1)]}$$

$$= \frac{2}{\pi}\cdot\int_0^{x_e}\left[\int_u^{x_e}\frac{\sqrt{x_e-t}}{\sqrt{t-u}}dt\cdot A_e''(u)\right]du \quad \text{(change the order of integration)}$$

$$= \frac{2}{\pi}\cdot\int_0^{x_e}\left[\frac{\pi}{2}\cdot(x_e-u)\cdot A_e''(u)\right]du \quad \text{[use substitution } t = u + \sin^2(\theta)\cdot(x_e-u)\text{]}$$

$$= (x_e-u)\cdot\int_0^u A_e''(t)\,dt\Big|_{u=0}^{u=x_e} + \int_0^{x_e}\left(\int_0^u A_e''(t)\,dt\right)du \text{ (use integration by parts)}$$
$$= \int_0^{x_e}\left(\int_0^u A_e''(t)\,dt\right)du = \int_0^{x_e}\left(A_e'(u) - A_e'(0)\right)du \text{ [use Eq. (3)]}$$
$$= A_e(x_e) - A_e(0) - A_e'(0)\cdot x_e = A_e(x_e) - A_e'(0)\cdot x_e \text{ [use Assumption (i)]}$$

In the above derivation, the change of integration order is based on Fubini's theorem [30] {see also page 164 in Ref. [28]}, which ensures that the integration order can be exchanged if the integrand is Lebesgue integrable. In particular, the integration order can be exchanged if $\int_0^{x_e} |A_e''(t)|/\sqrt{x_e-t}\,dt$ is bounded for $0 < x_e \le l_e$. The next equality is the evaluation of the inner integral using integration by substitution. The Lebesgue integrability of $A_e''(x)$ on [0, l_e] and Eq. (3) imply that $\int_0^x A_e''(t)dt$ is absolutely continuous for $x_e \le l_e$ and its derivative is $A_e''(x_e)$ except at finitely many locations. The conditions for validity of integration

by parts for less smooth functions in Ref. [31,32] are satisfied. So, the equality for integration by parts in the above derivation holds. The last two lines of equalities are based on Eq. (3) and Assumption (i). So, (1.2) of Theorem 1 holds.

Finally, (1.3) of Theorem 1 follows easily from (1.2) of Theorem 1. If $A_e'(0) = 0$, then $\boldsymbol{A}\circ\boldsymbol{F}(A_e) = A_e(x_e)$ for $x_e \le l_e$ follows from (1.2) of Theorem 1. On the other hand, if $\boldsymbol{A}\circ\boldsymbol{F}(A_e) = A_e(x_e)$ for $x_e \le l_e$, by (1.2) of Theorem 1, $A_e(x_e) - A_e'(0)\cdot x_e = A_e(x_e)$ for $x_e \le l_e$, which implies $A_e'(0) = 0$. This completes the proof of (1.3) of Theorem 1.

Remarks. **1)** The assumptions in Theorem 1 are given in such a way that they are satisfied by the equivalent areas converted from the F-functions that are continuous for $0 < x_e \le l_e$ with a potential jump discontinuity at $x_e = 0$. If $|A_e''(x_e)|$ is bounded for $x_e \le l_e$, then $\boldsymbol{F}(A_e)$ is continuous on $[0, l_e]$ and Assumptions (iv) and (v) are satisfied. In derivation of Eq. (2) from the inverse Abel transform of Eq. (1), Jones assumed the continuity of the first derivative of $\boldsymbol{F}(A_e)$ {see page 434 of Ref. [26]} for A_e due to lift and used the property $A_e'(0) = 0$ for A_e due to volume {see page 435 of Ref. [26]}. In comparison, the F-functions for sonic boom minimization in Ref. [3] have a jump discontinuity between 0 and l_e, in addition to a jump discontinuity at $x_e = 0$ when the corresponding ground signatures have flat-top shapes. It is still an open problem what mathematical properties of $A_e(x_e)$ are necessary and sufficient to ensure $\boldsymbol{A}\circ\boldsymbol{F}(A_e) = A_e(x_e)$ for $x_e \le l_e$.

2) Theorem 1 reveals the required boundary condition $A_e'(0) = 0$ for Eq. (2) to be the inverse transform of Eq. (1) for $x_e \le l_e$. In mathematics, the claim that Eq. (2) is the inverse transform of Eq. (1) is false if $A_e'(0) \ne 0$, which might be satisfied by a blunt-tipped projectile. If we further assume $A_e(x_e) = A_e(l_e)$ for $x_e > l_e$ in Eq. (1), then one can verify that $\boldsymbol{A}\circ\boldsymbol{F}(A_e) = A_e(x_e)$ for all x_e if and only if $A_e'(0) = A_e'(l_e) = 0$. Note that $A_e'(l_e) = 0$ is the necessary and sufficient condition for the continuity of $A_e'(x_e)$ as a function for all x_e under the assumptions of Theorem 1. In general, if $A_e'(x_e)$ has a jump discontinuity at a location between 0 and l_e, then Eq. (3) must account for the jump discontinuity in the right hand side and the inverse relation $\boldsymbol{A}\circ\boldsymbol{F}(A_e) = A_e(x_e)$ becomes invalid after the location of discontinuity.

3) In general, a jump discontinuity of $F(x)$ at $x = 0$ is due to a positive limit of $A_e''(x)\cdot x^{1/2}$ as x approaches zero. For example, if $A_e(x)$ is the sum of $\sigma\cdot x^{3/2}$ and a function with a continuous second derivative near $x = 0$, then $A_e''(x) \approx 3\sigma\cdot x^{-1/2}/4$ is unbounded near $x = 0$ and $F(x) = \boldsymbol{F}(A_e)$ has a jump discontinuity at $x = 0$ with the height of the jump being $(3\cdot\sigma)/8$. Any F-function for a flat-top pressure signature has a jump discontinuity at $x = 0$ [3,4]. The unboundedness of $A_e''(x)$ near $x = 0$ leads to slow convergence of any numerical formula to compute $\boldsymbol{F}(A_e)$.

4) The assumption for boundedness of $\int_0^{x_e} |A_e''(t)|/\sqrt{x_e - t}\, dt$ for $x_e > 0$ is important for applications. For example, if $A_e(x) = x^{5/4}$ near $x = 0$, then $A_e''(x) = 5x^{-3/4}/16$. So, for x close to 0, we have

$$F(x) = \frac{1}{2\pi}\cdot\int_0^x \frac{A_e''(t)}{\sqrt{x-t}}dt = \int_0^x \frac{5}{32\cdot\pi\cdot t^{\frac{3}{4}}\sqrt{x-t}}dt \ge \frac{1}{x^{\frac{1}{4}}}\cdot\int_0^x \frac{5}{32\cdot\pi\cdot t^{\frac{1}{2}}\sqrt{x-t}}dt = \frac{5}{32}\cdot x^{-\frac{1}{4}}$$

Because $F(x)$ is unbounded near $x = 0$, it cannot be used to predict the CFD pressure distribution around a supersonic configuration. The Whitham theory is invalid for such an equivalent area.

Theorem 2 (Inversion from Equivalent Area to Whitham's F-function). Assume that $F(x_e)$ is continuous and bounded for $0 < x_e \le l_e$, $F(0) = 0$, and $A_e = \boldsymbol{A}(F)$ satisfies Assumptions (iii)-(v) in Theorem 1. Then $\boldsymbol{F}\circ\boldsymbol{A}(F) = F$ for $x_e \le l_e$, i.e., Eq. (1) is also the inverse transform of Eq. (2) for $x_e \le l_e$.

Proof. Because $F(x)$ is continuous and bounded for $0 < x_e \le l_e$, we can differentiate Eq. (2) with respect to x_e using the Leibniz integral rule [33] {see also Ref. [34]}.

$$A'_{\mathrm{e}}(x_{\mathrm{e}}) = 4 \cdot F(t) \cdot \sqrt{x_{\mathrm{e}} - t}\,\big|_{t=x_{\mathrm{e}}} + 2 \cdot \int_0^{x_{\mathrm{e}}} \frac{F(t)}{\sqrt{x_{\mathrm{e}} - t}}\, dt$$
$$= 2 \cdot \int_0^{x_{\mathrm{e}}} \frac{F(t)}{\sqrt{x_{\mathrm{e}} - t}}\, dt = 2 \cdot \int_0^{x_{\mathrm{e}}} \frac{F(x_{\mathrm{e}} - u)}{\sqrt{u}}\, du \tag{4}$$

Because $F(x_{\mathrm{e}})$ is continuous and bounded for $0 < x_{\mathrm{e}} \le l_{\mathrm{e}}$, Eq. (4) implies that $A'_{\mathrm{e}}(x_{\mathrm{e}})$ is continuous for $x_{\mathrm{e}} \le l_{\mathrm{e}}$ with $A'_{\mathrm{e}}(0) = 0$. Equation (2) defines $A_{\mathrm{e}}(0) = 0$. Because all the assumptions in Theorem 1 are satisfied and $A'_{\mathrm{e}}(0) = 0$, we obtain $\boldsymbol{A}\circ\boldsymbol{F}(A_{\mathrm{e}}) = A_{\mathrm{e}}(x_{\mathrm{e}})$ for $x_{\mathrm{e}} \le l_{\mathrm{e}}$ [see (1.3) of Theorem 1]. Moreover, $\boldsymbol{F}(A_{\mathrm{e}})$ defined by Eq. (1) is bounded and continuous for $0 < x_{\mathrm{e}} \le l_{\mathrm{e}}$ [see (1.1) of Theorem 1]. Let $G = \boldsymbol{F}(A_{\mathrm{e}}) - F$. Then $\boldsymbol{A}(G) = \boldsymbol{A}\circ\boldsymbol{F}(A_{\mathrm{e}}) - \boldsymbol{A}(F) = A_{\mathrm{e}} - A_{\mathrm{e}} = 0$ for $x_{\mathrm{e}} \le l_{\mathrm{e}}$. Here the second equality follows from $\boldsymbol{A}\circ\boldsymbol{F}(A_{\mathrm{e}}) = A_{\mathrm{e}}$ and $A_{\mathrm{e}} = \boldsymbol{A}(F)$ for $x_{\mathrm{e}} \le l_{\mathrm{e}}$. As a result, we have

$$\boldsymbol{A}(G) = 4 \cdot \int_0^{x_{\mathrm{e}}} G(t) \cdot \sqrt{x_{\mathrm{e}} - t}\, dt = 0 \quad \text{for } x_{\mathrm{e}} \le l_{\mathrm{e}} \tag{5}$$

Because G is the difference of two bounded continuous functions $\boldsymbol{F}(A_{\mathrm{e}})$ and F for $0 < x_{\mathrm{e}} \le l_{\mathrm{e}}$, G is bounded and continuous for $0 < x_{\mathrm{e}} \le l_{\mathrm{e}}$. By differentiating Eq. (5) with respect to x_{e} using the Leibniz integral rule again, one derives

$$4 \cdot G(t) \cdot \sqrt{x_{\mathrm{e}} - t}\,\big|_{t=x_{\mathrm{e}}} + 2 \cdot \int_0^{x_{\mathrm{e}}} \frac{G(t)}{\sqrt{x_{\mathrm{e}} - t}}\, dt = 2 \cdot \int_0^{x_{\mathrm{e}}} \frac{G(t)}{\sqrt{x_{\mathrm{e}} - t}}\, dt = 0 \quad \text{for } 0 < x_{\mathrm{e}} \le l_{\mathrm{e}} \tag{6}$$

Let $g(x) = \int_0^x \int_0^t G(u)\, du\, dt$. Because G is a bounded continuous function for $x_{\mathrm{e}} > 0$, $g'(x) = \int_0^x G(u) dt$ is a continuous function. Moreover, $g''(x) = G(x)$ is a bounded continuous function for $x > 0$. Then Eq. (6) implies

$$\boldsymbol{F}(g) = \frac{1}{2\pi} \cdot \int_0^{x_{\mathrm{e}}} \frac{g''(t)}{\sqrt{x_{\mathrm{e}} - t}}\, dt = \frac{1}{2\pi} \cdot \int_0^{x_{\mathrm{e}}} \frac{G(t)}{\sqrt{x_{\mathrm{e}} - t}}\, dt = 0 \quad \text{for } 0 < x_{\mathrm{e}} \le l_{\mathrm{e}} \tag{7}$$

By the definition of $g(x)$, $g(0) = 0$. So, $g(x)$ satisfies all the assumptions in Theorem 1. It follows from (1.2) of Theorem 1 that

$$\boldsymbol{A}\circ\boldsymbol{F}(g) = g(x_{\mathrm{e}}) - g'(0) \cdot x_{\mathrm{e}} \qquad \text{for } x_{\mathrm{e}} \le l_{\mathrm{e}} \tag{8}$$

By Eq. (7), the left hand side of Eq. (8) is zero. So, Eq. (8) yields $g(x_{\mathrm{e}}) = g'(0) \cdot x_{\mathrm{e}}$ for $x_{\mathrm{e}} \le l_{\mathrm{e}}$, which implies $G(x_{\mathrm{e}}) = g''(x_{\mathrm{e}}) = 0$, i.e., $\boldsymbol{F}(A_{\mathrm{e}}) = F(x_{\mathrm{e}})$, for $0 < x_{\mathrm{e}} \le l_{\mathrm{e}}$. This completes the proof of Theorem 2.

Remarks. 1) In mathematics, $\boldsymbol{A}\circ\boldsymbol{F}$ being an identity operator does not necessarily imply that $\boldsymbol{F}\circ\boldsymbol{A}$ is also an identity operator. The proof of $\boldsymbol{F}\circ\boldsymbol{A}(F) = F$ requires the use of Theorem 1. Theorems 1 and 2 ensure that Eqs. (1) and (2) are inverse transforms of each other if $A'_{\mathrm{e}}(0) = 0$. For the equivalent areas and F-functions used in the GSD sonic boom minimization theory [3,4], one could analytically verify that the equivalent area without the $x^{1/2}$ term and the corresponding F-function are inverse transforms of each other using Eqs. (1) and (2). So, the GSD sonic boom minimization theory does not depend on the general inverse relations between Eqs. (1) and (2). The boundary condition $A'_{\mathrm{e}}(0) = 0$ is also satisfied in the extensions of the GSD F-functions for sonic boom minimization [35-38] because $A_{\mathrm{e}}(x_{\mathrm{e}})$ is defined using Eq. (2) [see the proof after Eq. (4)] with a continuous F-function on $[0, l_{\mathrm{e}}]$.

2) Unlike the direct verification method for $\boldsymbol{A}\circ\boldsymbol{F}(A_{\mathrm{e}}) = A_{\mathrm{e}}$ in Theorem 1, the above proof of $\boldsymbol{F}\circ\boldsymbol{A}(F) = F$ is highly non-intuitive. The reason is that an explicit form of $A''_{\mathrm{e}}(x_{\mathrm{e}})$ requires $F'(x_{\mathrm{e}})$, which might not exist. If $F(x_{\mathrm{e}})$ has a continuous first derivative, which is an assumption made by Jones on page 434 of Ref. [26] and

means empirically that the longitudinal pressure distribution has no shock, then one could use the Leibniz integral rule to get an expression for $A_e''(x_e)$ by differentiating Eq. (4) with respect to x_e.

$$\begin{aligned} A_e''(x_e) &= \frac{F(0)}{\sqrt{x_e}} + 2\cdot\int_0^{x_e} \frac{F'(x_e-u)}{\sqrt{u}}\,du \\ &= 2\cdot\int_0^{x_e} \frac{F'(x_e-u)}{\sqrt{u}}\,du = 2\cdot\int_0^{x_e} \frac{F'(u)}{\sqrt{x_e-u}}\,du \end{aligned} \qquad \text{for } x_e > 0 \qquad (9)$$

Then one could substitute A_e'' in Eq. (1) with the right-hand side of Eq. (9) to verify that the right hand side of Eq. (1) equals $F(x_e)$.

$$\begin{aligned} &\frac{1}{2\pi}\cdot\int_0^{x_e} \frac{A_e''(t)}{\sqrt{x_e-t}}\,dt \\ &= \frac{1}{2\pi}\cdot\int_0^{x_e} \left(2\cdot\int_0^{t} \frac{F'(u)}{\sqrt{t-u}}\,du\right)\frac{1}{\sqrt{x_e-t}}\,dt \quad \text{[use Eq. (9)]} \\ &= \frac{1}{\pi}\cdot\int_0^{x_e} \left[\int_u^{x_e} \frac{1}{\sqrt{x_e-t}\cdot\sqrt{t-u}}dt\right]\cdot F'(u)\,du \quad \text{(change the order of integration)} \\ &= \frac{1}{\pi}\cdot\int_0^{x_e} \pi\cdot F'(u)\,du \quad \text{(evaluate the inner integral using integration by substitution)} \\ &= F(x_e) - F(0) = F(x_e) \end{aligned}$$

3 Numerical Conversion from Equivalent Area to F-function

For numerical conversion from $A_e(x_e)$ to $F(x_e)$, let $0 = x_0 < x_1 < \ldots < x_n = l_e < \ldots < x_N$ be a partition of the interval $[0, x_N]$ with $N \geq n$. The desired property of the partition is that $A_e''(x_e)$ can be accurately approximated by a linear function on $x_{i-1} < x_e < x_i$ $(1 \leq i \leq n)$ and $F(x_e) \approx 0$ for $x_e > x_N$. Then, $F(x_k)$ for $0 < k \leq N$ can be computed using the following approximation formula.

$$F(x_k) = \frac{1}{2\pi}\cdot\int_0^{x_k} \frac{A_e''(t)}{\sqrt{x_k-t}}dt = \frac{1}{2\pi}\cdot\sum_{i=1}^{k}\int_{x_{i-1}}^{x_i} \frac{A_e''(t)}{\sqrt{x_k-t}}dt \approx \frac{1}{2\pi}\cdot\sum_{i=1}^{k}\int_{x_{i-1}}^{x_i} \frac{(t-x_i)\cdot\frac{\Delta A_i''}{\Delta x_i} + A_i''}{\sqrt{x_k-t}}dt \qquad (10)$$

Here $A_i'' \approx A_e''(x_i)$, $\Delta x_i = x_i - x_{i-1}$, $\Delta A_i'' = A_i'' - A_{i-1}''$ for $i \leq n$, and $\Delta A_i'' = 0$ for $i > n$. With these choices of parameters, the piecewise linear approximation is identical to zero on $[x_n, x_N]$, because $A_e''(x_e) = 0$ on $[x_n, x_N]$. Note that the numerical error in the computed value of $F(x_k)$ is caused by the numerical errors in the piecewise linear approximation of $A_e''(x_e)$. The integrals in the right-hand size of Eq. (10) can be computed exactly to get the following discrete numerical conversion from $A_e(x_e)$ to $F(x_e)$.

$$\begin{aligned} F(x_k) \approx{}& \frac{1}{3\pi}\cdot\sum_{i=1}^{k}\frac{\Delta A_i''}{\Delta x_i}\cdot\left((x_k-x_i)^{\frac{3}{2}} - (x_k-x_{i-1})^{\frac{3}{2}}\right) \\ &-\frac{1}{\pi}\cdot\sum_{i=1}^{k}\left((x_k-x_i)\cdot\frac{\Delta A_i''}{\Delta x_i} + A_i''\right)\cdot\left((x_k-x_i)^{\frac{1}{2}} - (x_k-x_{i-1})^{\frac{1}{2}}\right) \end{aligned} \qquad (11)$$

In application, the exact value of $A_e''(x_i)$ might not be available. The following numerical approximation of $A_e''(x_i)$ is used to define A_i''.

$$A_i'' = 2\cdot\frac{\left(\frac{A_e(x_{i+1})-A_e(x_i)}{x_{i+1}-x_i}\right)-\left(\frac{A_e(x_i)-A_e(x_{i-1})}{x_i-x_{i-1}}\right)}{x_{i+1}-x_{i-1}} \quad \text{for } 1 \le i \le n-1$$

$$A_0'' = 2\cdot\frac{A_e(x_1)}{(x_1)^2} \quad \text{if } A_e'(0)=0 \text{ or } A_0''=A_1'' \text{ if } A_e'(0)\neq 0 \tag{12}$$

$$A_n'' = 2\cdot\frac{A_e(x_{n-1})-A_e(l_e)}{(x_{n-1}-l_e)^2} \quad \text{if } A_e'(l_e)=0 \text{ or } A_n''=A_{n-1}'' \text{ if } A_e'(l_e)\neq 0$$

$$A_i'' = 0 \text{ for } i > n$$

In Eq. (12), only the values of $A_e(x_e)$ on $[0, l_e]$ are used to define A_i'' for the numerical conversion from $A_e(x_e)$ to $F(x_e)$. The special value of A_0'' is derived from the Taylor expansion $A_e(x_1) \approx A_e''(0)\cdot(x_1)^2/2$ using $A_e(0) = A_e'(0) = 0$. The expression for A_n'' is obtained similarly using $A_e'(l_e) = 0$. If $A_e'(0) = 0$ or $A_e'(l_e) = 0$ is violated, then a constant approximation of $A_e''(x_e)$ is used on the relevant subinterval. The value of the numerical approximation of $F(x_e)$ between the partition points can also be computed exactly.

$$\begin{aligned} F(x_e) \approx{}& \frac{1}{\pi}\cdot A_k''\cdot(x_e-x_{k-1})^{\frac{1}{2}} - \frac{1}{3\pi}\cdot\frac{\Delta A_k''}{\Delta x_k}\cdot(x_e-x_{k-1})^{\frac{3}{2}} + \frac{1}{3\pi}\cdot\sum_{i=1}^{k-1}\frac{\Delta A_i''}{\Delta x_i}\cdot\left((x_e-x_i)^{\frac{3}{2}}-(x_e-x_{i-1})^{\frac{3}{2}}\right) \\ & -\frac{1}{\pi}\cdot\sum_{i=1}^{k-1}\left((x_e-x_i)\cdot\frac{\Delta A_i''}{\Delta x_i}+A_i''\right)\cdot\left((x_e-x_i)^{\frac{1}{2}}-(x_e-x_{i-1})^{\frac{1}{2}}\right) \qquad \text{for } x_{k-1} < x_e \le x_k \end{aligned} \tag{13}$$

The numerical conversion from A_e to F defined by right-hand side of Eq. (13) is denoted by $\boldsymbol{F}_N(A_e)$. In theory, Eq. (13) is very different from the numerical conversion in Refs. [21,22], where the numerical approximation of $F(x_e)$ is a linear combination of $\sqrt{x_e - x_i}$ with $x_i \le x_e$ {see eq. (14) in Ref. [22]}. If one replaces the piecewise linear approximation of $A_e''(x_e)$ by a piecewise constant approximation of $A_e''(x_e)$, then the corresponding numerical conversion from $A_e(x_e)$ to $F(x_e)$ is what was proposed by Carlson [21]. The choice of the constant for a segment $[x_{i-1}, x_i]$ was not explicitly given in Ref. [21]. In Ref. [22], the central divided difference A_{i-1}'' is used to approximate $A_e''(x_e)$ on $[x_{i-1}, x_i]$. Equation (13) with $\Delta A_i'' = 0$ for all i becomes Carlson's formula for computing Whitham's F-function if A_i'' is used to approximate $A_e''(x_e)$ on $[x_{i-1}, x_i]$. The solution generated by Carlson's formula using $(A_{i-1}''+A_i'')/2$ as the constant approximation of $A_e''(x_e)$ on the subinterval $[x_{i-1}, x_i]$ will be called Carlson's average approximation of $\boldsymbol{F}(A_e)$. In application, Eq. (13) and Carlson's average approximation of $\boldsymbol{F}(A_e)$ generate nearly identical solutions.

Note that Jung, Starkey, and Argrow [39] preferred Lighthill's F-function to Whitham's F-function for predicting off-body pressure distributions of supersonic configurations. One reason is that a Riemann sum formula for numerical approximation of Whitham's F-function is sensitive to the grid density {see the paragraph after eq. (23) in Ref. [39]}. In theory, the Riemann sum formula should not be used as a numerical approximation of an improper integral, which defines Whitham's F-function. Equation (13) is not sensitive to the grid density as long as the maximum value of Δx_i is small enough (see Sec. 5). One can prove that the maximum approximation error in Eq. (13) approaches zero as the maximum value of Δx_i goes to zero if $A_e''(x_e)$ is continuous on $[0, l_e]$.

4 Numerical Conversion from F-function to Equivalent Area

Let $0 = x_0 < x_1 < \ldots < x_n = l_e < \ldots < x_N$ be a partition of the interval $[0, x_N]$ such that the values of $F(x_i)$ for $1 \le i \le N$ are available. Ideally, $F(x_e)$ can be accurately approximated by a linear function for each subinterval $x_{i-1} < x_e < x_i$ $(1 \le i \le N)$ and $F(x_e) \approx 0$ for $x_e > x_N$. Let $A_e(x_e) = \boldsymbol{A}(F)$ be the equivalent area for $F(x_e)$. Then, for $0 < k \le N$,

$$A_e(x_k) = 4\cdot\int_0^{x_k} F(t)\cdot\sqrt{x_k - t}\,dt = 4\sum_{i=1}^{k}\int_{x_{i-1}}^{x_i} F(t)\cdot\sqrt{x_k - t}\,dt$$
$$\approx 4\sum_{i=1}^{k}\int_{x_{i-1}}^{x_i}\left\{(t - x_i)\cdot\frac{\Delta F_i}{\Delta x_i} + F_i\right\}\cdot\sqrt{x_k - t}\,dt$$

Here $F_i = F(x_i)$, $\Delta F_i = F_i - F_{i-1}$, and $\Delta x_i = x_i - x_{i-1}$. The integrals in the above approximation formula can be computed exactly to obtain the following discrete numerical conversion from $F(x_e)$ to $A_e(x_e)$.

$$A_e(x_k) \approx \sum_{i=1}^{k}\frac{8}{5}\cdot\frac{\Delta F_i}{\Delta x_i}\cdot\left((x_k - x_i)^{\frac{5}{2}} - (x_k - x_{i-1})^{\frac{5}{2}}\right)$$
$$-\sum_{i=1}^{k}\frac{8}{3}\cdot\left((x_k - x_i)\cdot\frac{\Delta F_i}{\Delta x_i} + F_i\right)\cdot\left((x_k - x_i)^{\frac{3}{2}} - (x_k - x_{i-1})^{\frac{3}{2}}\right) \qquad \text{for } 1 \le k \le N \qquad (14)$$

The value for the numerical approximation of $A_e(x_e)$ between the partition points can also be computed exactly.

$$A_e(x_e) \approx \frac{8}{3}\cdot F_k\cdot(x_e - x_{k-1})^{\frac{3}{2}} - \frac{8}{5}\cdot\frac{\Delta F_k}{\Delta x_k}\cdot(x_e - x_{k-1})^{\frac{5}{2}} + \sum_{i=1}^{k-1}\frac{8}{5}\cdot\frac{\Delta F_i}{\Delta x_i}\cdot\left((x_e - x_i)^{\frac{5}{2}} - (x_e - x_{i-1})^{\frac{5}{2}}\right)$$
$$-\sum_{i=1}^{k-1}\frac{8}{3}\cdot\left((x_e - x_i)\cdot\frac{\Delta F_i}{\Delta x_i} + F_i\right)\cdot\left((x_e - x_i)^{\frac{3}{2}} - (x_e - x_{i-1})^{\frac{3}{2}}\right) \qquad \text{for } x_{k-1} < x_e \le x_k \qquad (15)$$

The numerical conversion from F to A_e defined by the right-hand side of Eq. (15) is denoted by $\boldsymbol{A}_N(F)$. One can prove mathematically that if $F(x_e)$ is continuous on $[0, l_e]$, then the maximum value of $|\boldsymbol{A}(F) - \boldsymbol{A}_N(F)|$ approaches zero as the maximum value of Δx_i goes to zero. The inverse relations $\boldsymbol{A}\circ\boldsymbol{F}(A_e) = A_e$ and $\boldsymbol{F}\circ\boldsymbol{A}(F) = F$ in Theorems 1 and 2 mean that, if $A_e''(x_e)$ and $F(x_e)$ are continuous on $[0, l_e]$ with $A_e'(0) = 0$, then the maximum values of $|A_e - \boldsymbol{A}_N\circ\boldsymbol{F}_N(A_e)|$ and $|F - \boldsymbol{F}_N\circ\boldsymbol{A}_N(F)|$ for $x_e \le l_e$ approach zero as the maximum value of Δx_i goes to zero.

5 Accuracy of Numerical Conversions

The purpose of this section is to study the numerical approximation errors $\boldsymbol{F}(A_e) - \boldsymbol{F}_N(A_e)$, $\boldsymbol{A}(F) - \boldsymbol{A}_N(F)$, $A_e - \boldsymbol{A}_N\circ\boldsymbol{F}_N(A_e)$, and $F - \boldsymbol{F}_N\circ\boldsymbol{A}_N(F)$ using three examples. The numerical evaluations of $\boldsymbol{F}_N(A_e)$ and $\boldsymbol{A}_N(F)$ are performed for the same set of discrete points $0 = x_0 < x_1 < \ldots < x_n = l_e < \ldots < x_N$. When possible, the following five constraints are used to select x_i: (i) $x_{n+1} = l_e + (l_e - x_{n-1})$, (ii) $x_N = 1.5\cdot l_e$, (iii) N is the closest integer to $4n/3$, (iv) $x_0 < \ldots < x_n$ are as equally spaced as possible, and (v) $x_{n+1} < \ldots < x_N$ are equally spaced. The choices of $x_{n+1} = l_e + (l_e - x_{n-1})$, $x_N = 1.5\cdot l_e$, and $N \approx 4n/3$ are empirical. The equal spacing constraints strive for approximately equal accuracies of piecewise linear approximations of $A_e''(x_e)$ and $F(x_e)$ over the interval $[x_0, x_N]$. The first example in Sec. 5.1 is an equivalent area for a body of revolution. This example represents a difficult case for approximating A_e'' by a piecewise linear function because $A_e''(x_e)$ is unbounded near $x_e = 0$. But $\boldsymbol{F}_N(A_e)$ converges to $\boldsymbol{F}(A_e)$ pointwise as N goes to infinity. The second example in Sec. 5.2 is an equivalent area target for low-boom inverse design optimization. Because A_e'' is a continuous function on $[0, l_e]$ and $A_e'(0) = 0$, for $F = \boldsymbol{F}(A_e)$, the numerical approximations $F \approx \boldsymbol{F}_N(A_e)$, $A_e \approx \boldsymbol{A}_N(F)$, $A_e \approx \boldsymbol{A}_N\circ\boldsymbol{F}_N(A_e)$, and $F \approx \boldsymbol{F}_N\circ\boldsymbol{A}_N(F)$ become very accurate with $n = 50$. To illustrate the importance of the boundary condition $A_e'(0) = 0$, A_e is modified slightly to satisfy $A_e'(0) \ne 0$. Then the numerical approximation $\boldsymbol{F}(A_e) \approx \boldsymbol{F}_N(A_e)$ is

still accurate, but the maximum value of $|A_e - \boldsymbol{A}_N \circ \boldsymbol{F}_N(A_e)|$ is about 5.7 even if $n = 4000$. The last example in Sec. 5.3 is a reversed equivalent area of a low-boom supersonic transport. It is used to show that the inverse relations between $\boldsymbol{F}_N$ and $\boldsymbol{A}_N$ [i.e., $A_e \approx \boldsymbol{A}_N \circ \boldsymbol{F}_N(A_e)$ and $F \approx \boldsymbol{F}_N \circ \boldsymbol{A}_N(F)$] are very accurate for discrete forms of F and A_e from an application in inverse design of low-boom supersonic aircraft.

5.1 Body of Revolution with Unbounded A_e''

Let $A_e(x) = x^{3/2} \cdot (x-100)^2/60000$ for $x \le 100$ ft and $A_e(x) = A_e(l_e) = 0$ for $x > l_e = 100$ ft (see Fig. 1a). Then $A_e(0) = A_e'(0) = A_e'(l_e) = 0$ and $A_e(x)$ can be considered as the equivalent area of a body of revolution with a length of 100 ft. Because $A_e''(x)$ is unbounded near $x = 0$, the piecewise linear approximation of $A_e''(x)$ has significant errors near $x = 0$. In this case, for $F = \boldsymbol{F}(A_e)$, one can verify analytically that the right limit of $F(x)$ is 1/16 as x goes to zero because $A_e(x) \approx x^{3/2}/6$ near $x = 0$ and $\boldsymbol{F}(x^{3/2}/6) = 1/16 = 0.0625$ for $x > 0$. So, $F(x)$ has a jump discontinuity at $x = 0$.

The equally spaced points $x_i = 100 \cdot i/n$ for $0 \le i \le n$ are used to define $\boldsymbol{A}_N$ and $\boldsymbol{F}_N$. Recall that $N \approx 4n/3$ is determined by n. The value of n indicates the partition resolution for the interval $[0, l_e]$ where the approximate values of $A_e''(x_i)$ are used for a piecewise linear approximation of $A_e''(x)$. So, the numerical results are labeled by the value of n instead of $N \approx 4n/3$.

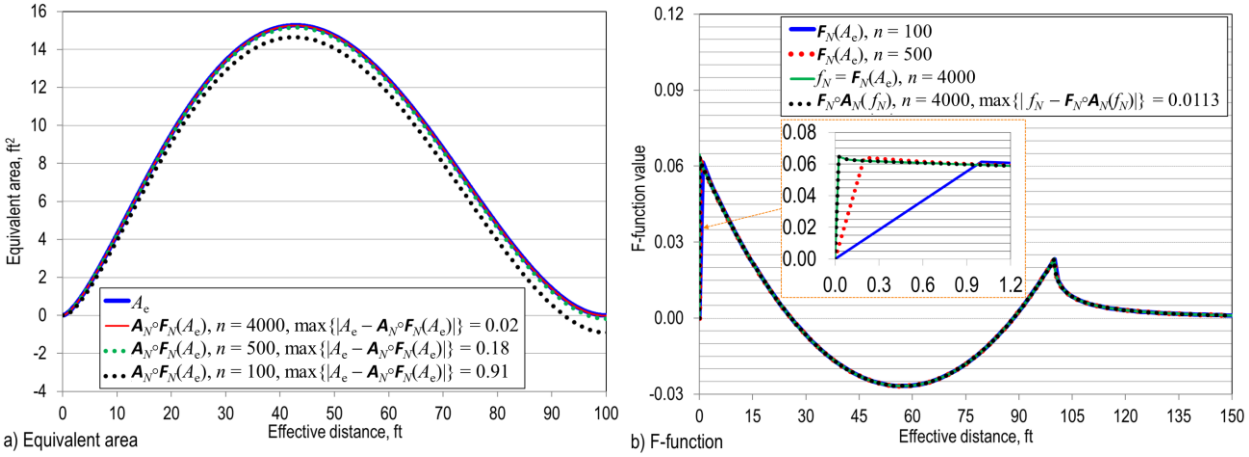

Fig. 1 Accuracy of numerical conversions between A_e and F for a body of revolution.

Figure 1a shows that the maximum error of $|A_e - \boldsymbol{A}_N \circ \boldsymbol{F}_N(A_e)|$ is significant when $n = 100$ (dotted black curve), but it is nearly zero when $n = 4000$ (red curve). Because the analytical formula of $\boldsymbol{F}(A_e)$ is not available, $f_N = \boldsymbol{F}_N(A_e)$ with $n = 4000$ (green curve in Fig. 1b) is used to verify the accuracy of $\boldsymbol{F}_N \circ \boldsymbol{A}_N$ as the identity transform. Figure 1b shows that the inversion error $|f_N - \boldsymbol{F}_N \circ \boldsymbol{A}_N(f_N)|$ for $n = 4000$ (dotted black curve) appears to be zero visually, but the maximum inversion error is 0.0113 due to a minor misalignment of the approximately vertical segments near $x_e = 0$. The values of $\boldsymbol{F}_N(A_e)$ are almost identical for $x_e > 1$ when $n \ge 100$. However, near $x_e = 0$, the values of $\boldsymbol{F}_N(A_e)$ change as n increases (see the zoomed view in Fig. 1b). The initial peak of $\boldsymbol{F}_N(A_e)$ moves toward the right limit of $F(x_e)$ at $x_e = 0$ as n increases. This example shows that Eq. (13) might be inaccurate near $x_e = 0$ if $A_e''(x_e)$ is unbounded near $x_e = 0$. Mathematically, it means that $\boldsymbol{F}_N(A_e)$ converges to $\boldsymbol{F}(A_e)$ for each fixed x_e as N goes to infinity, but the convergence is not uniform. Because $\boldsymbol{F}_N(A_e)$ is used to predict the off-body pressure for sonic boom analysis, $\boldsymbol{F}_N(A_e)$ for $n = 500$ (dotted red curve in Fig. 1b) is considered to be accurate enough if the grid spacing for CFD analysis in the longitudinal direction is more than 0.2% of l_e.

5.2 Equivalent Area Target for Low-Boom Inverse Design

The second $A_e(x)$ is a typical equivalent area target for low-boom inverse design of the reversed equivalent area of a supersonic transport [16,17]. For $0 \le t \le 1$, the corresponding point $(x, A_e(x))$ on a Bezier curve is defined as follows.

$$x(t) = \sum_{j=0}^{7} x_{c,j} \cdot \frac{7!}{j!\,(7-j)!} \cdot t^j \cdot (1-t)^{7-j}$$

$$A_e\big(x(t)\big) = \sum_{j=0}^{7} y_{c,j} \cdot \frac{7!}{j!\,(7-j)!} \cdot t^j \cdot (1-t)^{7-j}$$

Here $x_{c,0} = y_{c,0} = 0$, $x_{c,1} = 59.26$, $y_{c,1} = 0$, $x_{c,2} = 139.7$, $y_{c,2} = 8.503$, $x_{c,3} = 152.8$, $y_{c,3} = 247.1$, $x_{c,4} = 171.2$, $y_{c,4} = 175.9$, $x_{c,5} = 187.8$, $y_{c,5} = 221.1$, $x_{c,6} = 197.3$, $y_{c,6} = 225$, $x_{c,7} = 250$, and $y_{c,7} = 225$.

The locations $x_i = x(i/n)$ for $0 \le i \le n$ are used to define $\boldsymbol{A}_N$ and $\boldsymbol{F}_N$, where $x(i/n)$ is computed using the parametric formula for $x(t)$. One can verify that $A_e''(x)$ is continuous on $[0, l_e]$ with $l_e = 250$ ft and $A_e(0) = A_e'(0) = A_e'(l_e) = 0$. Define $A_e(x) = A_e(l_e)$ for $x > l_e$. Then, $A_e'(x)$ is a continuous function for all $x \ge 0$, $A_e''(x)$ exists everywhere except at $x = l_e$, and $|A_e''(x)|$ is bounded. All the required conditions for $A_e = \boldsymbol{A}\circ\boldsymbol{F}(A_e)$ in Theorem 1 are satisfied. In this case, the maximum error of $|A_e - \boldsymbol{A}_N\circ\boldsymbol{F}_N(A_e)|$ decreases from 0.22 [about 0.1% of $A_e(l_e)$] to 0.0003 when n increases from 50 to 4000 (compare dotted green and dotted black curves with blue curve in Fig. 2a), which confirms the inverse relation $A_e = \boldsymbol{A}\circ\boldsymbol{F}(A_e)$ computationally. Also, the curves of $\boldsymbol{F}_N(A_e)$ for $n \ge 50$ are nearly identical (compare dotted green curve with blue curve in Fig. 2b). As a result, $F = \boldsymbol{F}(A_e)$ is represented by $\boldsymbol{F}_N(A_e)$ with $n = 4000$ (blue curve in Fig. 2b) even though the exact values of F are not available. The inverse relation $F = \boldsymbol{F}\circ\boldsymbol{A}(F)$ is confirmed computationally by the maximum error of 0.00003 (i.e., 0.05% of the magnitude of F) for $|F - \boldsymbol{F}_N\circ\boldsymbol{A}_N(F)|$ with $n = 4000$ (compare dotted black curve with blue curve in Fig. 2b). However, if we use Eq. (12) with $A_0'' = A_1''$ and $A_n'' = A_{n-1}''$, then $\boldsymbol{A}_N\circ\boldsymbol{F}_N(A_e)$ for $n = 50$ (red curve in Fig. 2a) is visibly different from A_e (blue curve in Fig. 2a) with a maximum difference of 2.2. The four numerical solutions for $n = 50$ (red and dotted green curves in Fig. 2) imply that the linear approximations of $A_e''(x)$ on $[0, x_1]$ and $[x_{n-1}, l_e]$ yield more accurate $\boldsymbol{F}_N(A_e)$ and $\boldsymbol{A}_N\circ\boldsymbol{F}_N(A_e)$ than the constant approximations of $A_e''(x)$ on $[0, x_1]$ and $[x_{n-1}, l_e]$ when $A_e'(0) = A_e'(l_e) = 0$.

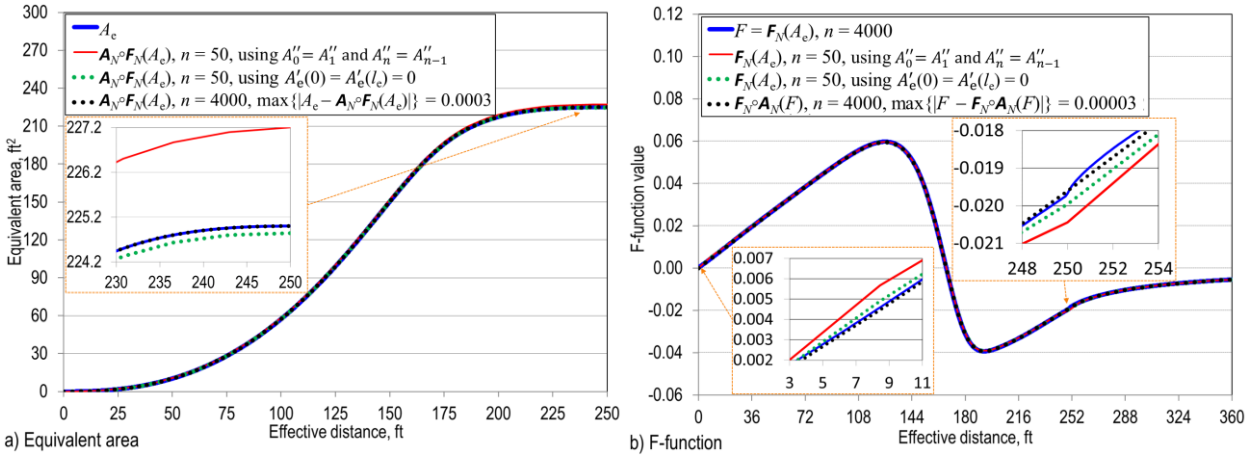

Fig. 2 Accuracy of numerical conversions between A_e and F for an equivalent area target.

If $A_e(x_e)$ in Fig. 2a is modified with $y_{c,1} = 1.35$ and $y_{c,6} = 224.55$, then $A_e'(0) = 0.02278$ and $A_e'(l_e) = 0.009$. In this case, (1.2) of Theorem 1 ensures $\boldsymbol{A}\circ\boldsymbol{F}(A_e) = A_e(x_e) - A_e'(0)\cdot x_e$ for $x_e \le l_e$, which is accurately approximated by $\boldsymbol{A}_N\circ\boldsymbol{F}_N(A_e)$ for $n = 400$ (green curve in Fig. 3a). The maximum value of $|A_e - \boldsymbol{A}_N\circ\boldsymbol{F}_N(A_e)|$ for

n = 4000 equals 5.695, which is $A'_e(0)\cdot l_e$ and agrees with (1.2) of Theorem 1 (see dotted black curve in Fig. 3a). Again, we can assume $F = \boldsymbol{F}_N(A_e)$ for n = 4000. Then $|f_N - \boldsymbol{F}_N \circ \boldsymbol{A}_N(f_N)|$ and $|f_N - F|$ are nearly zero for $f_N = \boldsymbol{F}_N(A_e)$ and n = 400 (compare dotted green, dotted black, and blue curves in Fig. 3b). The accuracy of the inverse relation $f_N \approx \boldsymbol{F}_N \circ \boldsymbol{A}_N(f_N)$ is guaranteed by Theorem 2 and the convergence of $\boldsymbol{F}_N(A_e)$ and $\boldsymbol{A}_N(F)$ to $\boldsymbol{F}(A_e)$ and $\boldsymbol{A}(F)$, respectively.

If we mistakenly use Eq. (12) assuming $A'_e(0) = A'_e(l_e) = 0$, which seems to be reasonable for the blue A_e curve in Fig. 3a, then $A_e \approx \boldsymbol{A}_N \circ \boldsymbol{F}_N(A_e)$ is relatively accurate for n = 400 (see dotted red curve in Fig. 3a). If one believed that $\boldsymbol{A} \circ \boldsymbol{F}(A_e) = A_e$ is always true, then $\boldsymbol{F}_N(A_e)$ with two spikes in Fig. 3b (red curve) would be considered as the most accurate approximation of $\boldsymbol{F}(A_e)$ among the solutions in Fig. 3b because $\boldsymbol{A}_N \circ \boldsymbol{F}_N(A_e)$ is significantly different from A_e for the other two F-function approximations. The two spikes in $\boldsymbol{F}_N(A_e)$ could represent the front and rear shocks for sonic boom minimization, similar to the features of the optimal F-functions in the GSD sonic boom minimization theory [3,4]. But the truth is that the two spikes in $\boldsymbol{F}_N(A_e)$ are due to the numerical conversion errors assuming $A'_e(0) = A'_e(l_e) = 0$. As the value of n increases, the width of each spike decreases and the height of each spike increases. The effects of such numerical errors in the conversion from A_e to F on the sonic boom analysis of A_e are beyond the scope of this paper. But such numerical errors could significantly affect the undertrack ground signature of A_e and need to be carefully studied.

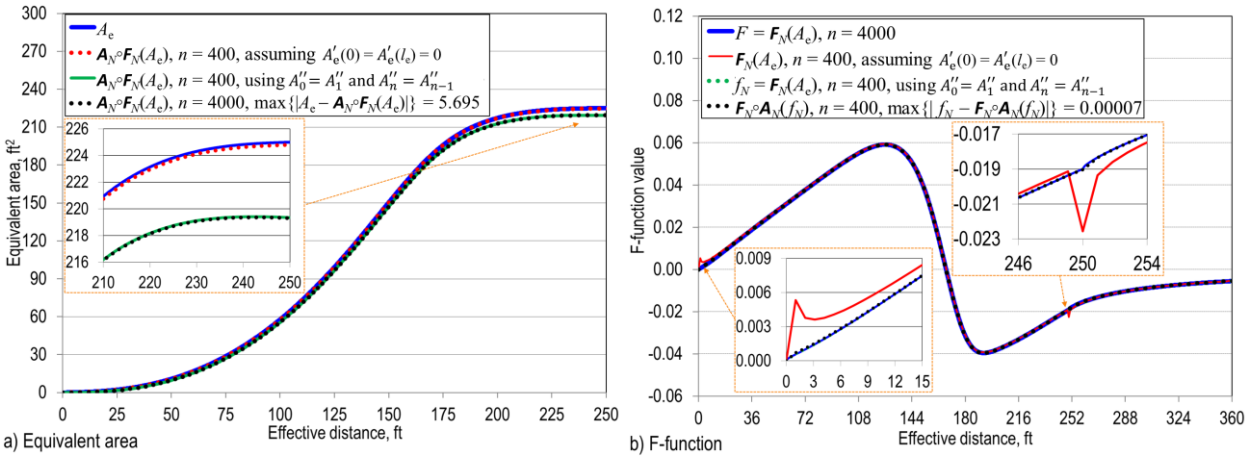

Fig. 3 Effects of $A'_e(0) \neq 0$ on the inverse relations between F-function and equivalent area.

5.3 Reversed Equivalent Area of a Low-Boom Supersonic Transport

The third $A_e(x_e)$ is the reversed equivalent area of the low-boom supersonic transport in Ref. [20]. This equivalent area represents a body of revolution that behaves like the low-boom supersonic transport for undertrack sonic boom analysis {see Ref. [18]}. Here we just show how $A_e(x_e)$ can be converted to Whitham's F-function and vice versa.

In this case, $F(x_e)$ is converted from an undertrack pressure distribution at 50 ft below the aircraft, which is obtained by reversely propagating the CFD undertrack pressure at three body lengths below the aircraft using an augmented Burgers equation [17]. Because the pressure distribution is continuous, $F(x_e)$ is considered as a continuous function.

The partition points of $0 = x_0 < x_1 < \ldots < x_N = 375$ ft with N = 524 are the locations where values of $F(x_i)$ for $0 \le i \le N$ are computed. The missing values of $F(x_e)$ between x_{i-1} and x_i are linearly interpolated using $F(x_{i-1})$ and $F(x_i)$. Then $A_e(x_e) = \boldsymbol{A}_N(F) = \boldsymbol{A}(F)$ satisfies $A'_e(0) = 0$ by the proof of Theorem 2. So, Eq. (12) is applied using $A'_e(0) = 0$. The effective length of the aircraft is 247.4 ft. But $F(x_e)$ does not represent the turbulent wake for a constant cross section when x_e > 247.4 ft. So, Eqs. (13) and (15) are applied with $l_e = x_N$ = 375 ft and $n = N$ = 524. Figure 4 shows that the approximations $F \approx \boldsymbol{F}_N \circ \boldsymbol{A}_N(F)$ and $A_e \approx \boldsymbol{A}_N \circ \boldsymbol{F}_N(A_e)$ are

very accurate, i.e., the inverse relations between $\boldsymbol{A}(\cdot)$ and $\boldsymbol{F}(\cdot)$ are well preserved by $\boldsymbol{A}_N(\cdot)$ and $\boldsymbol{F}_N(\cdot)$ in this case.

As mentioned before, $\boldsymbol{F}_N(A_e)$ and Carlson's average approximation of $\boldsymbol{F}(A_e)$ are nearly identical for the same set of x_i points, which has been confirmed by all the numerical comparison studies conducted. Figure 4a also includes Carlson's average approximation (dotted green curve) of $\boldsymbol{F}\circ\boldsymbol{A}_N(F)$ for comparison. The maximum absolute difference between $F(x_e)$ and Carlson's average approximation of $\boldsymbol{F}\circ\boldsymbol{A}_N(F)$ is 0.0037, which is slightly smaller than the maximum value of 0.0043 for $|F-\boldsymbol{F}_N\circ\boldsymbol{A}_N(F)|$.

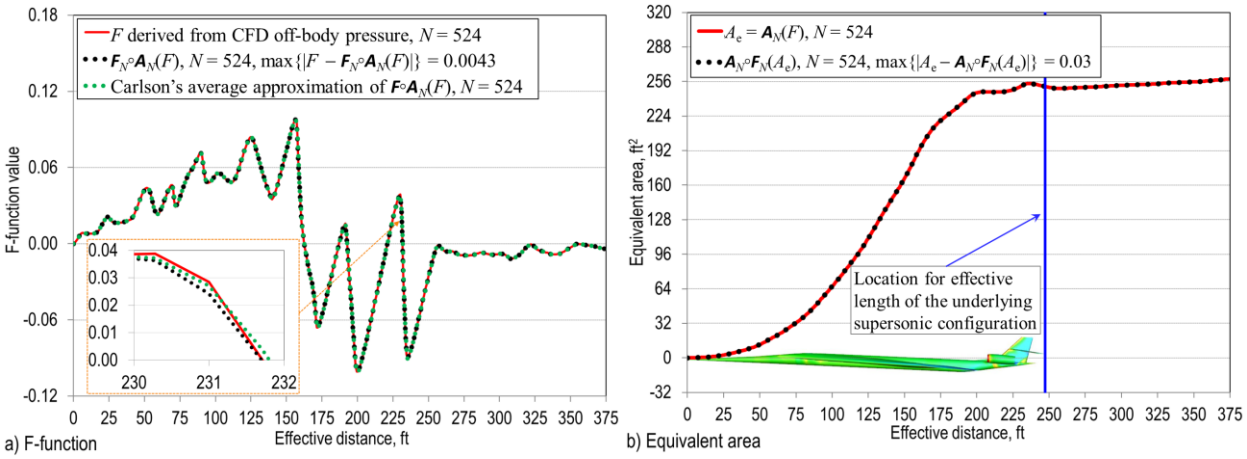

Fig. 4 Accuracy of numerical conversions between A_e and F for a reversed equivalent area.

6 Conclusions

For an equivalent area $A_e(x_e)$ and the corresponding Whitham's F-function $F(x_e)$, the inverse relations between the integral transforms between $A_e(x_e)$ and $F(x_e)$ are rigorously studied from mathematical and computational perspectives. The Whitham integral transform from $A_e(x_e)$ to $F(x_e)$ is denoted by $\boldsymbol{F}(A_e)$ and the inverse Abel transform from $F(x_e)$ to $A_e(x_e)$ is denoted by $\boldsymbol{A}(F)$. The necessary and sufficient boundary condition of A_e is derived for the validity of the inverse relations between $\boldsymbol{F}(A_e)$ and $\boldsymbol{A}(F)$. Under some general smoothness assumptions on A_e, $A_e = \boldsymbol{A}\circ\boldsymbol{F}(A_e)$ holds for $x_e \le l_e$ if and only if $A_e'(0) = 0$. This rigorously proved mathematical fact contradicts the accepted unconditional inverse relation between $\boldsymbol{F}(\cdot)$ and $\boldsymbol{A}(\cdot)$ in the sonic boom research literature. Explicit formulas are derived for numerical approximations of $\boldsymbol{F}(A_e)$ and $\boldsymbol{A}(F)$. The numerical approximations of $\boldsymbol{F}(A_e)$ and $\boldsymbol{A}(F)$ are very accurate when $A_e''(x_e)$ and $F(x_e)$ are continuous for $x_e \le l_e$. However, the numerical approximations of $\boldsymbol{A}\circ\boldsymbol{F}(A_e)$ converge to $A_e(x_e) - A_e'(0)\cdot x_e$ for $x_e \le l_e$ if $A_e'(0) \ne 0$, which confirms the proved theoretical result. The required boundary condition $A_e'(0) = 0$ for the inverse relation $A_e = \boldsymbol{A}\circ\boldsymbol{F}(A_e)$ and the numerical examples provide insight on the potential sources for numerical errors in the conversion from an equivalent area to the corresponding Whitham's F-function.

References

1. Whitham, G., "The Flow Pattern of a Supersonic Projectile," *Communications on Pure and Applied Mathematics*, Vol. 5, No. 3, 1952, pp. 301–348. doi:10.1002/cpa.3160050305
2. Whitham, G., "On the Propagation of Weak Shock Waves," *Journal of Fluid Mechanics*, Vol. 1, No. 3, 1956, pp. 290–318. doi:10.1017/S0022112056000172
3. Seebass, R., and George, A., "Sonic Boom Minimization," *Journal of the Acoustical Society of America*, Vol. 51, No. 2C, 1972, pp. 686–694. doi:10.1121/1.1912902

4. Darden, C., "Minimization of Sonic-Boom Parameters in Real and Isothermal Atmospheres," NASA TN D-7842, March 1975.

5. Pawlowski, J., Graham, D., Boccadoro, C., Coen, P., and Maglieri, D., "Origins and Overview of the Shaped Sonic Boom Demonstration Program," AIAA Paper 2005-5, January 2005. doi:10.2514/6.2005-5

6. Seebass, R., "Sonic Boom Theory," *Journal of Aircraft*, Vol. 6, No. 3, 1969, pp. 177–184. doi:10.2514/3.44032

7. Hayes, W., "Sonic Boom," *Annual Review of Fluid Mechanics*, Vol. 3, No. 1, 1971, pp. 269–290. doi:10.1146/ annurev.fl.03.010171.001413

8. Carlson, H., and Maglieri, D., "Review of Sonic-Boom Generation and Prediction Methods," *Journal of the Acoustical Society of America*, Vol. 51, No. 2C, 1972, pp. 676–685. doi:10.1121/1.1912901

9. Plotkin, K., "Review of Sonic Boom Theory," AIAA Paper 1989-1105, April 1989. doi:10.2514/6.1989-1105

10. Seebass, R., and Argrow, B., "Sonic Boom Minimization Revisited," AIAA Paper 1998-2956, June 1998. doi:10.2514/6.1998-2956

11. Plotkin, K., "State of the Art of Sonic Boom Modeling," *The Journal of the Acoustical Society of America*, Vol. 111, No. 1, 2002, pp. 530–536. doi:10.1121/1.1379075

12. Plotkin, K., and Maglieri, D., "Sonic Boom Research: History and Future," AIAA Paper 2003-3575, June 2003. doi:10.2514/6.2003-3575

13. Maglieri, D., Bobbitt, P., Plotkin, K., Shepherd, K., Coen, P., and Richwine, D., *Sonic Boom: Six Decades of Research*, NASA SP-2014-622, NASA Langley Research Center, 2014.

14. Park, M., and Carter, M., "Low-Boom Demonstrator Near-Field Summary for the Third AIAA Sonic Boom Prediction Workshop," *Journal of Aircraft*, Vol. 59, No. 3, 2022, pp. 563–577. doi:10.2514/1.C036323

15. Rallabhandi, S., and Loubeau, A., "Summary of Propagation Cases of the Third AIAA Sonic Boom Prediction Workshop," *Journal of Aircraft*, Vol. 59, No. 3, 2022, pp. 578–594. doi:10.2514/1.C036327

16. Chapman, K., "The X Factor—QueSST Exclusive," *Air International*, Sep. 2022, pp. 28–39.

17. Li, W., and Rallabhandi, S., "Inverse Design of Low-Boom Supersonic Concepts Using Reversed Equivalent-Area Targets," *Journal of Aircraft*, Vol. 51, No. 1, 2014, pp. 29–36. doi:10.2514/1.C031551

18. Li, W., "Equivalent Area Targets for Inverse Design Optimization with Changing Low-Boom Cruise Conditions," *AIAA Journal*, Vol. 61, No. 3, 2023, pp. 1260–1269. doi:10.2514/1.J062324

19. Li, W., and Geiselhart, K., "Integration of Low-Fidelity MDO and CFD-Based Redesign of Low-Boom Supersonic Transports," *AIAA Journal*, Vol. 59, No. 10, 2021, pp. 3923–3936. doi:10.2514/1.J060368

20. Li, W., and Geiselhart, K., "Multi-objective, Multidisciplinary Optimization of Low-Boom Supersonic Transports Using Multifidelity Models," *Journal of Aircraft*, Vol. 59, No. 5, 2022, pp. 1137–1151. doi:10.2514/1.C036656

21. Carlson, H., "Influence of Airplane Configuration on Sonic-Boom Characteristics," *Journal of Aircraft*, Vol 1, No. 2, 1964, pp. 82–86. doi:10.2514/3.43562

22. Igoe, W., "Application of Richardson's Extrapolation to Numerical Evaluation of Sonic-Boom Integral," NASA TN D-3806, March 1967.

23. Ritzel, D., and Gottlieb, J., "Numerical Evaluation of Whitham's F-function for Supersonic Projectiles," *AIAA Journal*, Vol. 26, No. 2, 1988, pp. 244–247. doi:10.2514/3.9880

24. Walkden, F., "The Shock Pattern of a Wing-Body Combination, Far from the Flight Path," *Aeronautical Quarterly*, Vol. 9, No. 2, 1958, pp. 164–194. doi:10.1017/S0001925900001372

25. De Micheli, E., "A Fast Algorithm for the Inversion of Abel's Transform," *Applied Mathematics and Computation*, Vol. 301, 2017, pp.12–24. doi:10.1016/j.amc.2016.12.009

26. Jones, L., "Lower Bounds for Sonic Bangs," *The Aeronautical Journal*, Vol. 65, No. 606, 1961, pp. 433–436. doi:10.1017/S0368393100074757

27. "Lebesgue Integration," Wikipedia, URL:https://en.wikipedia.org/wiki/Lebesgue_integration [retrieved 26 Oct. 2022].

28. Rudin, W., *Real and Complex Analysis*, Third Edition, McGraw-Hill Book Company, 1987.

29. "Fundamental Theorem of Calculus," Wikipedia, URL:https://en.wikipedia.org/wiki/Fundamental_theorem_of_calculus [retrieved 26 Oct. 2022].

30. "Fubini's Theorem," Wikipedia, URL:https://en.wikipedia.org/wiki/Fubini%27s_theorem [retrieved 26 Feb. 2022].

31. "Integration by Parts," Wikipedia, URL:https://en.wikipedia.org/wiki/Integration_by_parts [retrieved 26 Feb. 2022].

32. Pfeffer, W., "Integration by Parts for the Generalized Riemann-Stieltjes Integral," *Journal of the Australian Mathematical Society*, Vol. 34, No. 2, 1983, pp. 229–233. doi:10.1017/S1446788700023259

33. "Leibniz Integral Rule," Wikipedia, URL:https://en.wikipedia.org/wiki/Leibniz_integral_rule [retrieved 26 Feb. 2022].

34. Osgood, W., "On the Differentiation of Definite Integrals," *Annals of Mathematics*, Second Series, Vol. 9, No. 3, 1908, pp. 119–233. doi:10.2307/1967454

35. Rallabhandi, S., and Mavris, D., "Sonic Boom Minimization Using Inverse Design and Probabilistic Acoustic Propagation," *Journal of Aircraft*, Vol. 43, No. 6, 2006, pp. 1815–1828. doi:10.2514/1.20457

36. Plotkin, K., Rallabhandi, S., and Li, W., "Generalized Formulation and Extension of Sonic Boom Minimization Theory for Front and Aft Shaping," AIAA Paper 2009-1052, January 2009. doi:10.2514/6.2009-1052

37. Haas, A., and Kroo, I., "A Multi-Shock Inverse Design Method for Low-Boom Supersonic Aircraft," AIAA Paper 2010-843, June 2010. doi:10.2514/6.2010-843

38. Darden, C., "Sonic-Boom Minimization with Nose-Bluntness Relaxation," NASA TP-1348, January 1979.

39. Jung, T., Starkey, R., and Argrow, B., "Modified Linear Theory Sonic Booms Compared to Experimental and Numerical Results," *Journal of Aircraft*, Vol. 52, No. 6, 2015, pp. 1821–1837. doi:10.2514/1.C033088